

# Large-Scale Parallel Finite Element Analyses of High Frequency Electromagnetic Field in Commuter Trains

A. Takei<sup>1</sup>, S. Yoshimura<sup>1</sup> and H. Kanayama<sup>2</sup>

**Abstract:** This paper presents large-scale finite element analyses of high frequency electromagnetic fields in commuter trains. The ADVENTURE\_Magnetic is one of the main modules of the ADVENTURE system, which is an open source parallel finite element analyses system, and is able to solve eddy current and magnetostatic problems using the hierarchical domain decomposition method (HDDM) with an iterative linear algebraic solver. In this paper, we improve the module so as to solve a high frequency electromagnetic field of 500-1000 M[Hz]. A stationary Helmholtz equation for electromagnetic wave problems is solved taking an electric field as an unknown function. In this study, stable convergence is achieved by adding a stability term. Basic performance of the module is first investigated by solving a simple model. Then a part of a commuter train with seats, handrails and two human bodies is precisely modeled into a large-scale finite element mesh with Nedelec elements of about 5.2 million degrees of freedom (DOFs). The results prove that the improved module can predict precisely the distribution of the electromagnetic field produced by mobile phones inside commuter trains.

**Keyword:** ADVENTURE system, Large-scale analyses, Finite element method, HDDM, Environmental electromagnetic field.

## 1 Introduction

We are doing a research on the parallel finite element analyses technique for high frequency electromagnetic fields aiming at contributing to the risk assessment of the impact of such fields in a

living environment [Selmaoui, B. and Tuitou, Y. (1995)] [Toropainen, A. (2003)]. In order to perform such risk assessment, digital data regarding the electromagnetic field intensity need to have highest possible resolution. Also, the living environment used in the analyses model needs to be modeled as a whole. Various materials like dielectrics, metals, etc. of different shapes and sizes are contained in the model data. Moreover, in order to ensure sufficient calculation accuracy, it is necessary to set the maximum length of an element size to 1/10 of the wavelength of the electromagnetic field. Large-scale calculation is needed due to the complexity of the model.

In high frequency electromagnetic field analyses, the FDTD (Finite difference time domain) method, in which simulations can be intuitively performed by discretizing the physical expression of electromagnetic wave propagation within Yee's grid, is often used [Luebbers, R.J. and Langdon, H.S. (1996)] [Anzaldi, G. and Silva, F. et al. (2007)]. However, when a calculation model is created based on an actual living environment, which has to be modeled in detail, its calculation scale becomes prohibitively large. Therefore, it is believed that the finite element method, in which boundary conformity should be assured by an unstructural grid, is more desirable[Fujitsu Ltd. Poynting homepage].

There are commercial and open source electromagnetic field analyses software based on the finite element method. Commercial software mainly deals with the analyses of commercial frequency bands or electromagnetic fields produced by equipments like motors or transformers [JRI Solutions Ltd. JMAG homepage] [SSIL Ltd. EMSolutoin homepage]. Open-source software, such as a large-scale electromagnetic

<sup>1</sup> The University of Tokyo, Bunkyo-ku, Tokyo, Japan

<sup>2</sup> Kyushu University, Nishi-ku, Fukuoka, Japan

field analyses module ADVENTURE\_Magnetic, which is one of the modules of the large-scale finite element analyses system ADVENTURE, has been successfully used for various analyses [ADVENTURE project homepage] [Ogino, M. and Mukaddes, A.M.M. et al. (2004)]. On the other hand, there are a lot of reports about an analyses of high-frequency bands [Vouvakis, N.M. and Lee, J.F. (2004)] [Bertazzi, F. and Cappelluti, F. et al. (2006)] [Bleszynski, E. and Bleszynski, M. et al. (2004)]. However, to the best of our knowledge, no simulation using large-scale models constituted by complex shapes and many different materials have been reported up to this moment. Some simulation involving complex shapes, such as parabolic antennas, has been realized using commercial packages. However, these calculations are done using a single or a small number of processors and are limited to hundreds of thousands of DOFs [Ansoft Ltd. Homepage] [Photon Ltd. Homepage].

In this study, we are considering the large-scale parallel finite element analyses of high frequency electromagnetic fields in a living environment. The electromagnetic field considered in this research is of the order of hundreds to thousands of MHz. Modeling is done by solving Maxwell's equations, including the displacement current, and by using finite element analyses. Since large-scale computation is needed, we employ the ADVENTURE\_Magnetic module as a platform and improve it so as to solve high frequency electromagnetic fields. In order to deal with large-scale calculation, parallel implementation is realized using the hierarchical domain decomposition method (HDDM). Stable convergence of the conjugate orthogonal conjugate gradient (COCG) method is achieved by adding a stability term. In this paper, a part of a commuter train with seats, handrails and two human bodies is precisely modeled into a large-scale finite element mesh with Nedelec elements of about 5.2 million DOFs. The results clearly demonstrate that the improved module can predict the distribution of the electromagnetic field produced by mobile phones inside commuter trains.

## 2 Algorithm for parallel computing formulation

### 2.1 Helmholtz equation

Let  $\Omega$  be a domain with the boundary  $\partial\Omega$ . The Helmholtz equation which describes an electromagnetic field with single angle frequency  $\omega$  [rad/s] is drawn from the Maxwell's equations containing the displacement current [Soares Jr, D. and Vinagre, M.P. (2008)] [Young, D.L. and Ruan, J.W. (2005)] [Reitich, F. and Tamma, K.K. (2004)]. The Helmholtz equations describing an electric field  $\mathbf{E}$  [V/m] are given by (1a) and (1b), using the current density  $\mathbf{J}$  [A/m<sup>2</sup>] and the electric field  $\mathbf{E}$  by making  $j$  into an imaginary unit:

$$\text{rot}(1/\mu_r \text{rot}\mathbf{E}) - k_0^2 \epsilon_r \mathbf{E} = j\omega\mu_0 \mathbf{J} \quad \text{in } \Omega \quad (1a)$$

$$\mathbf{E} \times \mathbf{n} = \mathbf{0} \quad \text{on } \partial\Omega \quad (1b)$$

where  $\epsilon_0$  and  $\mu_0$  are the vacuum permittivity [F/m] and permeability [H/m], and  $\epsilon_r$  and  $\mu_r$  are the relative permittivity and permeability, respectively.  $k_0$  represents the wave number ( $= \omega\sqrt{\mu_0\epsilon_0}$ ) [Chen, R.S. and Ping, X.W. et al. (2006)].

In this analyses code, the electric field  $\mathbf{E}$  and the magnetic field  $\mathbf{H}$  are calculated. The Poynting vector, which represents the energy density of the electromagnetic field, is then obtained from the calculated  $\mathbf{E}$  and  $\mathbf{H}$ . Solving equation (1a), by imposing the boundary condition of (1b), we calculate the electric field  $\mathbf{E}$ . The magnetic field  $\mathbf{H}$  [A/m] is calculated from the computed electric field  $\mathbf{E}$  by post-processing using equation (2), which is one of Maxwell's equations. Finally, the time average value of the Poynting vector  $\langle \mathbf{S} \rangle$  [W/m<sup>2</sup>] is calculated by equation (3):

$$\text{rot}\mathbf{E} - j\omega\mu_0\mu_r\mathbf{H} = \mathbf{0} \quad (2)$$

$$\langle \mathbf{S} \rangle = \text{Re} \left[ \frac{1}{2} \mathbf{E} \times \overline{\mathbf{H}} \right] \quad (3)$$

### 2.2 Finite element formulation

In this section we describe the finite element approximation. The electric field  $\mathbf{E}$  are approximated with Nedelec elements (edge elements) [Golias, N.A. and Antonopoulos, C.S. et al. (1998)]. The finite element approximation

is as follows [Kanayama, H. and Tagami, D. et al. (2000)] [Kanayama, H. and Shioya, R. et al. (2002)] [Taeyoung, H. and Sangwon S. et al. (2006)].

Find  $\mathbf{E}_h$  such that

$$(1/\mu_r \text{rot} \mathbf{E}_h, \text{rot} \mathbf{E}_h^*) - (k_0^2 \epsilon_r \mathbf{E}_h, \mathbf{E}_h^*) - (j\omega \mu_0 \tilde{\mathbf{J}}_h, \mathbf{E}_h^*) = 0 \quad (4)$$

where  $(*,*)$  denotes the complex valued  $L^2$ -inner product and  $\tilde{\mathbf{J}}_h$  is a corrected excitation current density in a finite element analyses [Kanayama, H. and Sugimoto, S. (2006)]. Following the discretization using the finite element method, the following system of simultaneous linear equations is obtained:

$$Ku = f \quad (5)$$

where  $K$  denotes the coefficient matrix,  $u$  the unknown vector, and  $f$  the known right hand side.

This formulation is based on Maxwell's equations, in which the displacement current, that cannot be disregarded in high frequency electromagnetic field analyses, is contained. The electric field  $\mathbf{E}$ , which is not usually taken into consideration in conventional eddy current analyses, as in the ADVENTURE\_Magnetic module, is also calculated. When the matrix  $K$  is not diagonally dominant, convergence of iterative calculations gets worse. In such a case, convergence is improved by adding a stability term to the left hand side of equation (1a).

### 3 Algorithm for parallel computing

#### 3.1 Iterative domain decomposition method

We introduce an iterative domain decomposition method. The domain is partitioned into non-overlapping subdomains. The linear system (5) is rewritten as follows:

$$\begin{bmatrix} K_{II} & K_{IB} & K_{IE} \\ K_{BI} & K_{BB} & K_{BE} \\ K_{EI} & K_{EB} & K_{EE} \end{bmatrix} \begin{Bmatrix} u_I \\ u_B \\ u_E \end{Bmatrix} = \begin{Bmatrix} f_I \\ f_B \\ f_E \end{Bmatrix} \quad (6)$$

where the subscripts  $I$ ,  $B$ ,  $E$  correspond to the nodal points in the interior of the subdomains, on the interface boundary, and on the essential

boundary, respectively. Equation (6) leads to the following linear systems:

$$K_{II}u_I = f_I - K_{IB}u_B - K_{IE}u_E \quad (7)$$

$$\begin{aligned} & (K_{BB} - K_{BI}K_{II}^\dagger K_{IB})u_B \\ & = f_B - K_{BI}K_{II}^\dagger f_I - (K_{BE} - K_{BI}K_{II}^\dagger K_{IE})u_E \end{aligned} \quad (8)$$

where  $K_{II}^\dagger$  is a generalized inverse of  $K_{II}$ .

At first, the unknown vector  $u_B$  is obtained from the application of the following algorithm based on the COCG (Conjugate orthogonal conjugate gradient) method to equation (8) [Kanayama, H. and Sugimoto, S. (2006)]:

Choose  $u_B^0$ ;

Compute  $u_I^0$  by

$$(K_{II} \ K_{IB} \ K_{IE}) (u_I^0 \ u_B^0 \ u_E^0)^T = f_I;$$

$$p^0 = g^0 = (K_{BI} \ K_{BB} \ K_{BE}) (u_I^0 \ u_B^0 \ u_E^0)^T - f_B;$$

for  $n = 0, 1, \dots$ ;

compute  $p_I^n$  by

$$(K_{II} \ K_{IB} \ K_{IE}) (p_I^n \ p^n \ 0)^T = 0$$

$$q^n = (K_{BI} \ K_{BB} \ K_{BE}) (p_I^n \ p^n \ 0)^T;$$

$$\alpha^n = r^n \cdot r^n / p^n \cdot q^n;$$

$$u_B^{n+1} = u_B^n - \alpha^n p^n;$$

$$r^{n+1} = r^n - \alpha^n p^n$$

If  $\|r^{n+1}\| < \delta \|r^n\|$ , break;

$$\beta^n = r^{n+1} \cdot r^{n+1} / r^n \cdot r^n;$$

$$p^{n+1} = r^{n+1} + \beta^n p^n;$$

end;

where  $\|\cdot\|$

is the Euclidean norm and  $\delta$  is a positive constant. Because the matrix  $K_{II}$  is block diagonal corresponding to each subdomain, the vectors  $u_I^0$  and  $p_I^0$  can be solved independently in each subdomain. After solving  $u_B$ , the unknown function  $u_I$  is obtained from equation (7). The vector  $u_I$  is solved by the COCG method with a preconditioner, and can also be solved independently in each subdomain. Hence, we can get the unknown  $u$  in the whole domain.

### 3.2 Hierarchical domain decomposition method

The original domain is hierarchically divided into parts, which are further decomposed into smaller domains called subdomains (Fig.1). This is called the hierarchical domain decomposition method (HDDM). This is one of techniques for parallel computing. HDDM has some modes depending on roles of processors.

#### 3.2.1 Hierarchical Processor Mode

Hierarchical processor mode (H-mode) [Yoshimura, S. and Shioya, R. et al. (2002)] classifies processors into three groups, “Grand Parent,” “Parent,” and “Child.” One of the processors is assigned as Grand Parent, a few as Parent, and others as Child. The number of processors assigned as Parent is the same as that of parts. The number of Child processors can be varied; and it affects parallel performance.

The role of Grand Parent is to organize all processor communications (i.e., message passing) which occur between all processors. Parents prepare mesh data, manage finite-element analyses (FEA) results, and coordinate the COCG iteration, including the convergence decision for the COCG iteration. Parents send data to Child processors, where FEA is performed in parallel. After the FEA, Child processors send the results to Parents. This computation will be repeated until the COCG iteration is converged (Fig.2(a)).

#### 3.2.2 Parallel Processor Mode

The traditional HDDM was introduced in the previous section. However, because most communication time is taken between Parent processors and Child processors, the communication speed becomes important. Although the communication performance has also been improved in network technology in recent years, high-speed network is still expensive. On the other hand, for PC clusters generally used, the network speed becomes a bottleneck to the processing performance of the CPU. Moreover, when parallel processing performance is considered, it is important to reduce the amount of communications as much as possible.

Therefore, the Parent-only type (Parallel processor mode P-mode) is more useful than the H-mode [Kanayama, H. and Sugimoto, S. (2006)].

In the P-mode, Parent processing performs the FEA by themselves, which is computed by Child processors in the H-mode (Fig.2(b)). Although Parent processors store some of subdomain analyses data and coordinate the COCG iteration as a main work, the idling time of CPU increases in the H-mode, because of less computation in Parent processors. On the other hand, since all processors perform the FEA and CPU can be used without idleness in an environment with 10-20 CPUs, the P-mode is considered superior to the H-mode. In the P-mode, the numbers of Parent processors should be equal to that of parts.

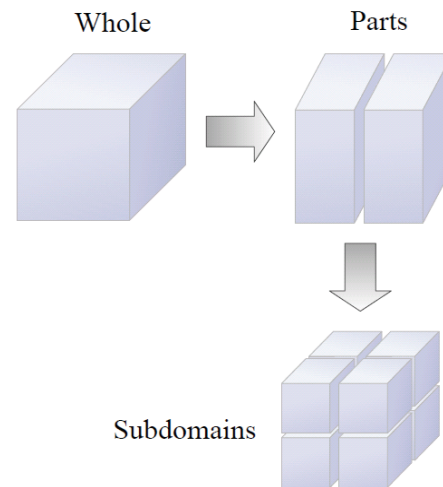
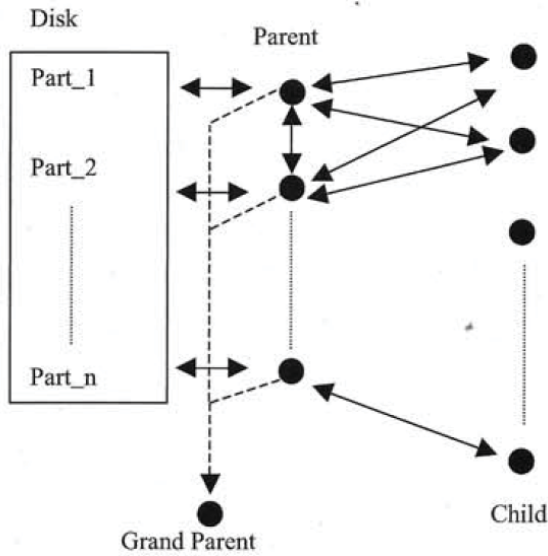


Figure 1: Hierarchical domain decomposition.

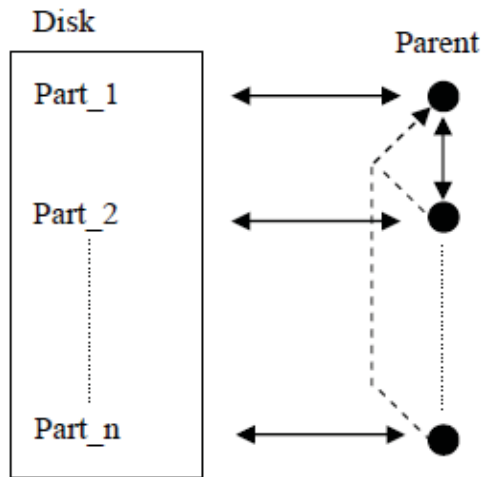
## 4 Verification

### 4.1 Verification model

In this study, a simple model, shown in Fig.3, is used for accuracy verification. The mesh is divided using Nedelec elements. The maximum size of element edge length is 0.03[m]. The permittivity is  $8.85 \times 10^{-12}$ [F/m]. The permeability is  $1.26 \times 10^{-6}$  [H/m]. The angular frequency is  $2\pi \times 500 \times 10^6$ [rad/s]. The absolute value of the real (or imaginary) part of the input current density  $|\mathbf{J}_r|$  (or  $|\mathbf{J}_i|$ ) in the antenna is 0.08 (or 0)



(a) Hierarchical processor mode.



(b) Parallel processor mode.

Figure 2: Data flow of HDDM.

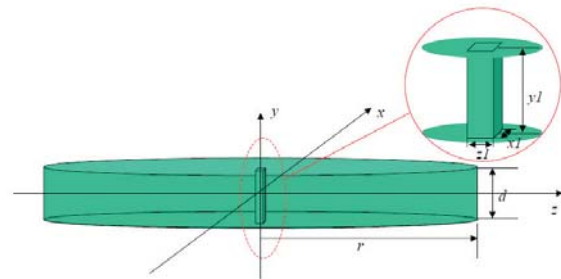
[A/m<sup>2</sup>]. Dirichlet boundary conditions of  $\mathbf{E} \times \mathbf{n} = \mathbf{0}$  are given on all surfaces. The number of DOFs is 381,022 and the number of elements is 269,224.

A simplified block diagonal scaling is used as the preconditioner in the COCG procedure on the interface. Each process is stopped when the residual norm  $\|r^n\| / \|r^0\|$

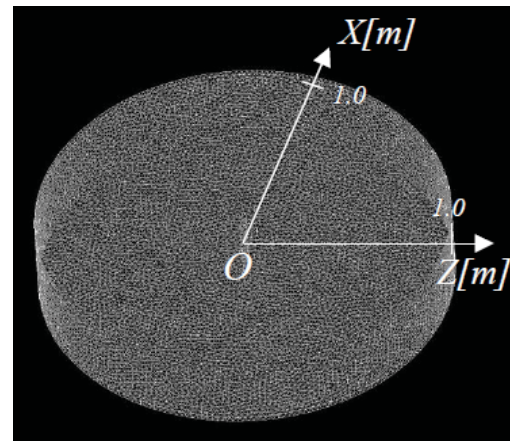
becomes less than  $10^{-3}$ . In each subdomain, the incomplete Cholesky conjugate orthogonal conjugate gradient (ICCOCG) method is used as the solver for the complex symmetric (not Hermitian)

system arising in approximations. The ICCOCG method in each subdomain is stopped when the preconditioned residual norm becomes less than  $10^{-10}$ .

The computation was performed by using 12 Intel Pentium 4 2.6-GHz processors. Fig.4 shows the history of the residual norms. The CPU time is 0.3 [h] and the number of elapsed iterations is 1680.



(a) Sketch of the model



(b) Mesh

Figure 3: Analytical model for verifications

#### 4.2 Comparison between the obtained numerical solution and the reference

We compared the numerical solution with a reference solution. The reference solution of the magnetic field  $\mathbf{H}$  on the  $x$ - $z$  plane surface ( $y=0$ )

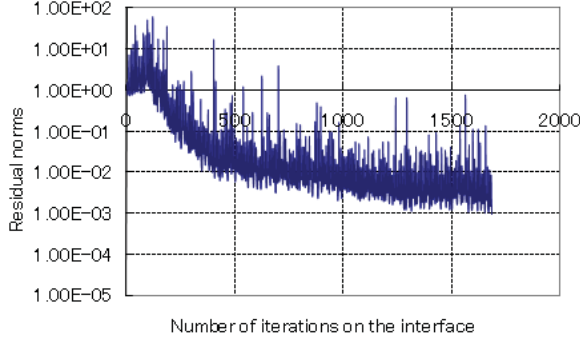


Figure 4: History of residual norms

is given by equation (9).

$$\begin{cases} \mu H_x = \frac{e^{-j\omega\sqrt{x^2+z^2}\sqrt{\mu\epsilon}} y J_{y,z}}{4\pi(x^2+z^2)^{3/2}} + j \frac{e^{-j\omega\sqrt{x^2+z^2}\sqrt{\mu\epsilon}} y J_{y,z} \omega \sqrt{\mu\epsilon}}{4\pi(x^2+z^2)} \\ \mu H_y = 0 \\ \mu H_z = -\frac{e^{-j\omega\sqrt{x^2+z^2}\sqrt{\mu\epsilon}} y J_{y,x}}{4\pi(x^2+z^2)^{3/2}} - j \frac{e^{-j\omega\sqrt{x^2+z^2}\sqrt{\mu\epsilon}} y J_{y,x} \omega \sqrt{\mu\epsilon}}{4\pi(x^2+z^2)} \end{cases} \quad (9)$$

This equation is compared with the numerical solution. The correlation coefficient  $CC$  between this reference solution  $\mathbf{H}_a$  and the numerical one  $\mathbf{H}_b$  is given by equation (10).

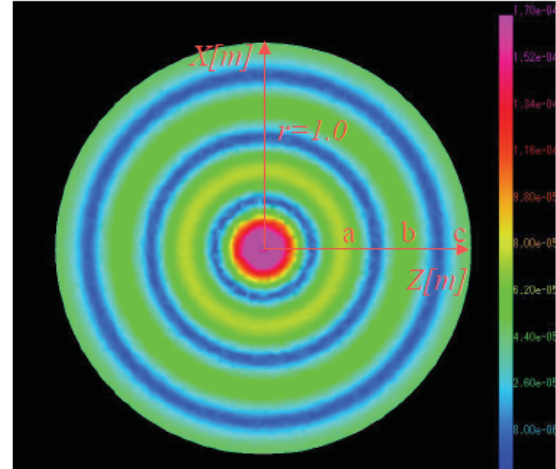
$$CC = \frac{\mathbf{H}_a \cdot \mathbf{H}_b}{|\mathbf{H}_a| |\mathbf{H}_b|} \times 100[\%] \quad (10)$$

The numerical solution and the reference are shown in Figs.5(a) and (b), respectively. These plots by the  $x$ - $z$  plane look identical. In both figures a, b, and c show the peak positions. It can be seen from the figures that both waveforms are in good agreement. Moreover, the correlation coefficient is  $CC=99$  [%]. In this study, the visualization tool is based on ADVENTURE AutoGL [Kawai H. (2006)].

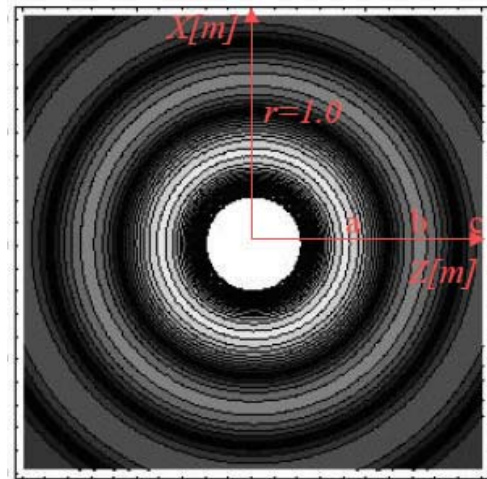
## 5 Real world application

### 5.1 Analyses

For examining the model and the proposed software on a real world problem, we model the environment of a commuter train, including two human bodies placed inside it. In such commuter



(a) A numerical result



(b) Reference solution

Figure 5: A numerical result and the reference solution

train, dielectrics, such as reflecting barriers, walls, handrails, etc. and human bodies exist. The electromagnetic field distribution may change with the differences of geometric arrangement between these materials. Therefore, when developing the numerical environmental model used for calculation, it is necessary to perform the modeling in such a way that the real environment may be reproduced correctly. The train plan [Monthly TRAIN (2004)] is referred for the modeling of the train. The CAD data were obtained by reading this plan using OCR (Optical Character Recognition) and by applying corrections where needed. The side view and the cross section of the CAD

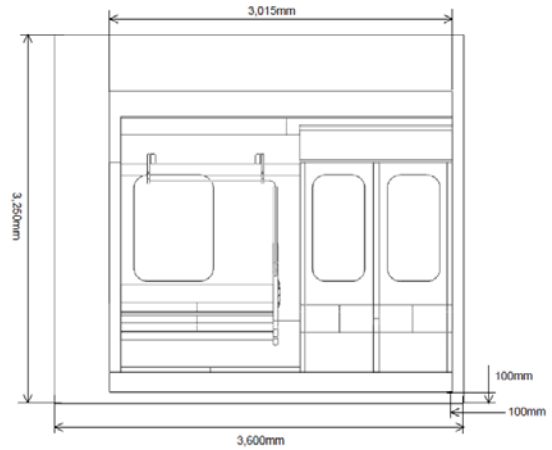
model are shown in Figs.6(a) and (b), respectively. Both dielectrics, like train parts made of plastic or rubber, and reflective parts like metals, which exist in a real commuter train, are contained in this model. Two human body models were added to this CAD data. The CAD model containing the two human bodies is shown in Fig.6(c). One person is sitting on a seat, while the other person is standing. The standing person is talking on a cellular phone which it holds in his hand. The electromagnetic field source is the cylinder type wave source which imitates a cellular phone. In this study, the human body composition was approximated by water. Moreover, the seats and the partition boards beside the seats were considered to be plastic. Metals are considered to be perfect conductors, and the basic boundary conditions from equation (1b) are applied [Takei, A. and Yoshimura, S. et al. (2006)]. The surface patch of the geometric model shown in Fig.7(a) was generated and element division was done by using Nedelec elements. The mesh is shown in Figs.7(b) and (c). The maximum size of element edge length is 0.0375 [m]. The number of DOFs is 5,235,812 and the number of elements is 4,330,480. Table 1 shows the material parameters.

Table 1: Material properties

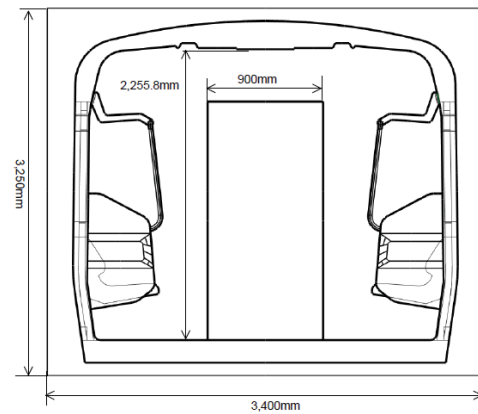
	Permeability [H/m]	Permittivity [F/m]
Air	$1.257 \times 10^{-6}$	$8.854 \times 10^{-12}$
Seat	$1.257 \times 10^{-6}$	$2.036 \times 10^{-11}$
Human bodies	$1.257 \times 10^{-6}$	$4.427 \times 10^{-11}$

### 5.2 Analyses

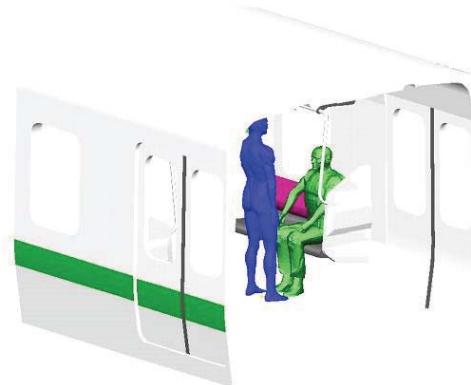
The electromagnetic fields are analyzed by the numerical environmental model shown in Fig.7. The angular frequency is  $2\pi \times 300 \times 10^6$  [rad/s]. The absolute value of the real (or imaginary) part of the input current density  $|\mathbf{J}_r|$  (or  $|\mathbf{J}_i|$ ) in the antenna is 0.08 (or 0) [A/m<sup>2</sup>]. Computation was performed using 17 dual core CPUs (34 processor elements) using Intel Core2Duo 1.86-GHz processors. Fig.8 shows the history of the residual



(a) Side view



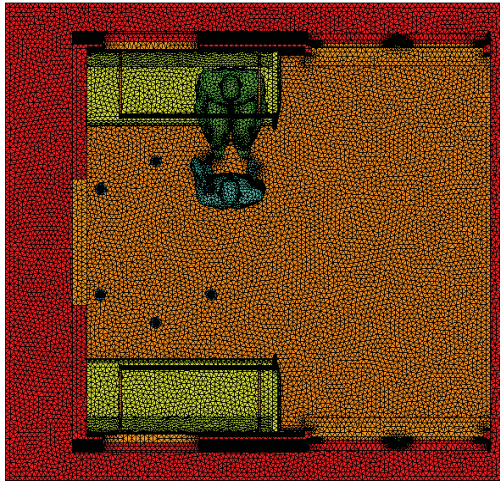
(b) Cross section



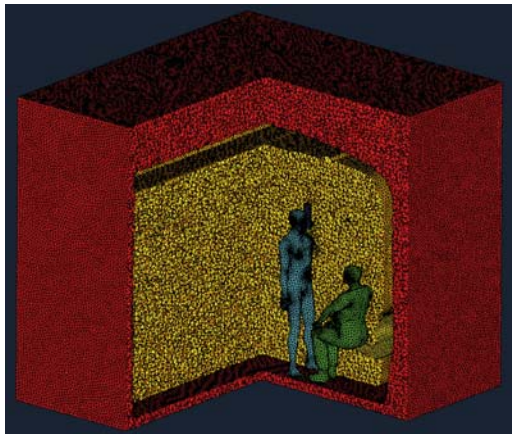
(c) CAD model including 2 human bodies

Figure 6: CAD model from OCR data.

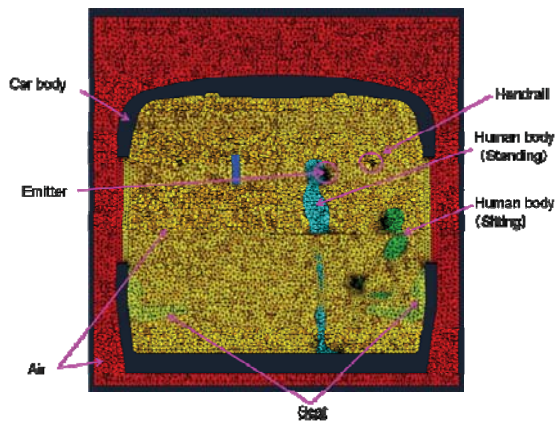
norms. The COCG calculation of the interface diverged after around 8000 iterations. Hence, the calculation could not be completed. Thus, this is a case where the system matrix, resulting from the particular shapes and arrangement of both metals



(a) Surface patches



(b) Mesh



(c) Each part in the mesh

Figure 7: Numerical model based on the CAD model.

and dielectrics placed inside the analyzed space, is not diagonally dominant. The convergence of the iterative COCG calculation between domains may get worse.

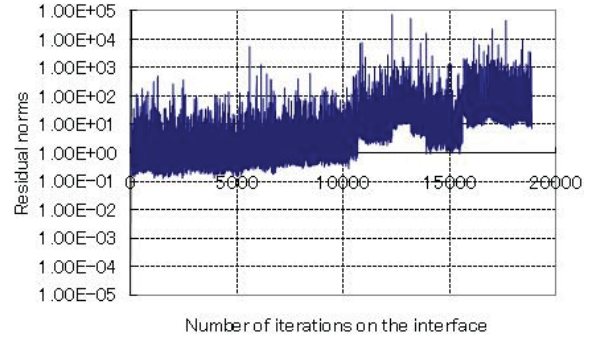


Figure 8: Residual norm of COCG iteration.

### 5.3 A stability term

A stability term is introduced in this calculation and the improvement of convergence in the iterative COCG calculation between domains is tried. A non-negative parameter  $e$  is introduced in equation (1a), and which takes the following form (11).

$$\text{rot}(1/\mu_r \text{rot}\mathbf{E}) - k_0^2 \epsilon_r \mathbf{E} - je\mathbf{E} = j\omega\mu_0 \mathbf{J}_0 \quad (11)$$

By adding the third term in the left hand side of equation (1a), the matrix to be solved becomes diagonally dominant, leading to an improvement in the convergence of the iterative COCG calculation of the interface. The addition of this stability term is one of the key ideas in this research. This stability term is computed by changing the current density  $\mathbf{J}$  of the right hand side equation (11).

$$\mathbf{J} = \mathbf{J}_0 + \mathbf{J}_{\text{ohm}} \quad (12a)$$

$$\mathbf{J}_{\text{ohm}} = \sigma \mathbf{E} \quad (12b)$$

Equation (12b) is Ohm's law.  $\sigma$  is the electrical conductivity [S/m]. Equation (11) is obtained from equations (12a) and (12b), (1a), and  $\omega\mu_0\sigma = e$ . The computation is now performed using the newly obtained equation (11). We search the value for the parameter  $e$  by starting

from  $e = 2.0 \times 10^{-12}$  ( $\sigma = 10^{-15}$ ) and further increasing this value over a number of steps ( $e = 2.0 \times 10^{-12}$  ( $\sigma = 10^{-15}$ ),  $2.0 \times 10^{-11}$  ( $\sigma = 10^{-14}$ ), etc.). The COCG converged for  $e = 0.2$  ( $\sigma = 10^{-4}$ ). Total CPU time was 9 [h]. Fig.9 shows the history of the residual norms.

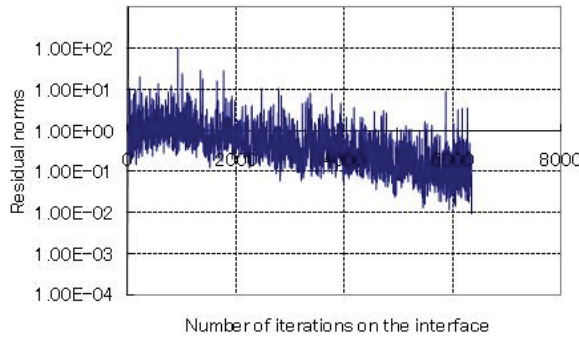


Figure 9: Residual norm of COCG iteration.

The influence to the solution and convergence properties of the parameter  $e = 0.2$  is investigated. Using the model for verification, shown in Fig.3, we compare solutions with the existence of a stability term. The norm of the magnetic fields on the X-axis shown in Fig.3 (b) is compared. Both comparisons are shown in Fig.10.

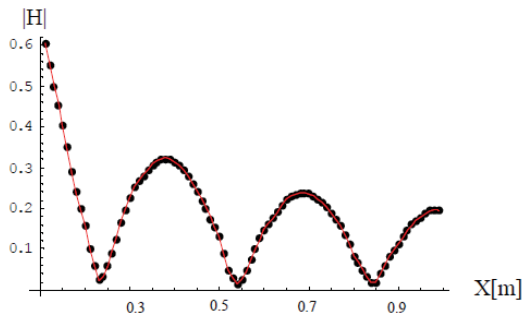


Figure 10: Solid and dotted lines show computed solutions with the stability term and without the stability term, respectively.

The result (magnetic field intensity) is shown in Fig.11. The numerical value shown in Fig.11 is the norm of the magnetic field vector  $\mathbf{H}$  [A/m]. Moreover, peaks are observed near the handrail (shown in Fig.11 by A), at metal boundaries (B), and at the cellular phone.

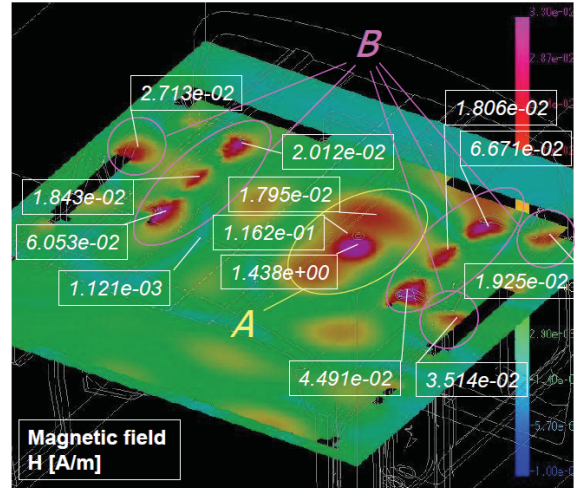


Figure 11: Magnetic fields in the commuter train.

## 6 Conclusions

In this paper, an examination of the techniques used for analyzing high frequency electromagnetic fields propagating in the environment of a commuter train has been performed. A new electromagnetic field analyses code is developed, which improves the existing ADVENTURE\_Magnetic module. The equation to be solved is the Helmholtz equation which is obtained from Maxwell's equations by including the displacement current. The problem formulation using finite element analyses and a parallel computational algorithm are described. A comparison between the reference solution and the obtained numerical solution is performed, which proves that the numerical solution is physically accurate. Moreover, an application to a real-world problem is considered by taking a commuter train as the environmental model. The modeling is done based on real schematics. In this computation, convergence is improved using a stability term. This example of high frequency electromagnetic field analyses, of frequency of around 300 M[Hz], in a commuter train, is done using a large-scale numerical environmental model of about 5 million DOFs.

## References

- Selmaoui, B.; Touitou, Y.** (1995): Sinusoidal 50-Hz Magnetic Fields Depress Rat NineaL NAT Activity and Serum Melatonin. Role of Duration and Intensity of Exposure. *Life Science*, vol.57, pp.1351-1358.
- Toropainen, A.** (2003): Human Exposure by Mobile Phones in Enclosed Areas. *Bioelectromagnetics*, vol.24, pp.63-65.
- Luebbers, R.J.; Langdon, H.S.** (1996): A Simple Feed Model That Reduces Time Step Needed for FDTD Antenna and Microstrip Calculations. *IEEE Trans. Antennas Propag.*, vol.44, pp.1000-1004.
- Anzaldi, G.; Silva, F.; Fernandez, M.; Quiez, M.; Riu, P.J.** (2007): Initial Analysis of SAR From a Cell Phone Inside a Vehicle by Numerical Computation. *IEEE Trans. on Biomed. Eng.*, vol.54, pp.921-930.
- Vouvakis, N.M.; Lee, J.F.** (2004): A Fast Non-Conforming DP-FETI Domain Decomposition Method for the Solution of Large EM Problems. *In Proc. IEEE Int. Antennas and Propagation Symp.*, vol.1, pp.623-626.
- Bertazzi, F.; Cappelluti, F.; Guerrieri, S.D.; Bonani, F.; Ghione, G.** (2006): Self-Consistent Coupled Carrier Transport Full-Wave EM Analysis of Semiconductor Traveling-Wave Devices. *IEEE Trans. Microw. Theory Tech.*, vol.54, pp.1611-1618.
- Bleszynski, E.; Bleszynski, M.; Jaroszewicz, T.** (2004): Development of New Algorithms for High Frequency Electromagnetic Scattering. *CMES: Computer Modeling in Engineering & Sciences*, vol.15, no.2, pp. 295-318
- Ogino, M.; Mukaddes, A.M.M.; Shioya, R.; Kanayama, H.** (2004): Large Scale Thermal-Solid Coupling Finite-Element Analysis with ADVENTURE System on Massively Parallel Computer. *In Proc. 4th Eur. Congr. Comput. Methods Appl. Sci.. Eng.*, vol.2, (CD-ROM).
- Soares Jr , D.; Vinagre, M.P.** (2008): Numerical Computation of Electromagnetic Fields by the Time-DomainBoundary ElementMethod and the Complex Variable Method. *CMES: Computer Modeling in Engineering & Sciences*, vol.25, no.1, pp.1-8.
- Young , D.L.; Ruan, J.W.** (2005): Method of Fundamental Solutions for Scattering Problems of Electromagnetic Waves. *CMES: Computer Modeling in Engineering & Sciences*, vol.7, no.2, pp.223-232.
- Reitich, F.; Tamma, K.K.** (2004): State-of-the-Art, Trends, and Directions in Computational Electromagnetics. *CMES: Computer Modeling in Engineering & Sciences*, vol.5, no.4, pp.287-294.
- Chen, R.S.; Ping, X.W.; Yung, E.K.N.; Chan, C. H.; Nie, Z.; Hu, J.** (2006): Application of Diagonally Perturbed Incomplete Factorization Preconditioned Conjugate Gradient Algorithms for Edge Finite-Element Analysis of Helmholtz Equations. *IEEE Trans. on Antennas and Propag.*, vol.54, pp.1604-1608.
- Kanayama, H.; Shioya, R.; Tagami, D.; Matsumoto, S.** (2002): 3-D Eddy Current Computation for a Transformer Tank. *International Journal for Computation and Mathematics in Electrical and Electronic Engineering(COMPEL)*, vol.21, pp.554-562.
- Golias, N.A.; Antonopoulos, C.S.; Tsiboukis, T.D.; Kriezis, E.E.** (1998): 3D eddy current computation with edge elements in terms of the electric intensity. *International Journal for Computation and Mathematics in Electrical and Electronic Engineering(COMPEL)*, vol.17, pp. 667 - 673.
- Taeyoung H.; Sangwon S.; Dongwoo S.** (2006): Parallel Iterative Procedures for a Computational Electromagnetic Modeling Based on a Nonconforming Mixed Finite Element Method. *CMES: Computer Modeling in Engineering & Sciences*, vol.14, no.1, pp.57-76.
- Kanayama, H.; Sugimoto, S.** (2006): Effectiveness of A- $\phi$  Method in a Parallel Computing with an Iterative Domain Decomposition Method. *IEEE Trans. Mag.*, vol.42, pp.539-542.
- Kanayama, H.; Tagami, D.; Saito, M.; Kikuchi, F.** (2000): A Finite Element Analysis of 3-D Eddy Current Problems Using an Iterative Method. *Transaction of JSCES*, Paper no.20000033, pp.201-208.
- Yoshimura, S.; Shioya, R.; Noguchi, H.; Miya-**

**mura, T.** (2002): Advanced General-Purpose Computational Mechanics System for Large Scale Analysis and Design. *Journal of Computational and Applied Mathematics*, vol.149, pp.279-296.

**Kawai, H.** (2006): ADVENTURE AutoGL: A Handy Graphics and GUI Library for Researchers and Developers of Numerical Simulations. *CMES: Computer Modeling in Engineering & Sciences*, vol.11, no.3, pp.111-120.

**Takei, A.; Yoshimura, S.; Dennis, B.H.; Kanayama, H.** (2006): Parallel FEM Analysis of High Frequency Electromagnetic Wave in an Environment. *Computational Methods*, Liu G.R., Tan V.B.C., Han X. Eds., Springer, pp.1587-1594.

**Monthly TRAIN** (2004), *Eriei press*, vol.357. (in Japanese)

**Fujitsu Ltd. Poynting** homepage,

<http://jp.fujitsu.com/solutions/plm/analysis/poynting/>

**JRI Solutions Ltd. JMAG** homepage,

<http://jmag.jri-sol.co.jp/en/index.html>

**SSIL Ltd. EMSolutoin** homepage,

<http://www.ssil.com/em/EMSolution/ja/index.html>

**ADVENTURE project** homepage,

<http://adventure.q.t.u-tokyo.ac.jp>

**Ansoft Ltd.** Homepage,

<http://www.ansoft.com/>

**Photon Ltd.** Homepage,

<http://www.photon-cae.co.jp/photon/jp/main2.html>

